Core precession: flow structures and energy

J. P. Vanyo and J. R. Dunn

Departments of Mechanical and Environmental Engineering, and Geological Sciences, University of California, Santa Barbara, CA 93106, USA.
E-mail: vanyo@engineering.ucsb.edu

SUMMARY

Experiments using a precessing liquid-filled oblate spheroid with ellipticity $(a-b)/a = 1/400$ extend and clarify earlier research. They yield flow data useful for estimating flows in the Earth's liquid core. Observed flows illustrate and confirm a nearly rigid liquid sphere with retrograde drift and lagging a cavity (mantle) axis in precession. The similarities of the observed lag angle with that computed for a rigid sphere, and earlier energy dissipation research both support the use of a rigid sphere analytical model to predict energy dissipation and first-order flow within the core–mantle boundary (CMB). Second-order boundary layer and interior cylindrical flow structures also are photographed and measured. Interior flows are never turbulent or unstable at near-Earth parameters, although complex and transient flow patterns are observed within the boundary layer. Other mechanisms proposed to explain net heat loss from the Earth and maintenance of the geodynamo typically require acceptance of some critical but unproven premise. Precession and CMB configuration are known with certainty and precision. Analytical difficulties have been the obstacle. Experiments illustrate the consequences of precession and ellipticity, provide criteria for validating analytical and numerical models, and may yield direct knowledge of the Earth's deep interior with careful scaling.

Key words: core–mantle boundary, Earth's core, fluid dynamics, geomagnetism, precession, terrestrial heat.

1 INTRODUCTION

Previous research on the ability of luni-solar precession of the mantle to induce flows in the Earth's liquid core is well documented. In the 1960s, research by Roberts & Stewartson (1965), Malkus (1968) and Busse (1968) yielded only modest success because of the intrinsic analytical difficulty of the problem, although that research and some preliminary experiments by Malkus showed promise. In the early 1970s, this research was criticized, leading researchers to seek other mechanisms to explain the geodynamo and net heat loss from the Earth (see e.g. Rochester *et al.* 1975; Loper 1975). Again, however, the intrinsic difficulty of the problem limited the critics mostly to discussions of previous attempts at analysis rather than thorough examinations of the concept.

Space travel was having its first successes during the same decades. Funding was abundant, with an emphasis on finding useful solutions to problems. One problem encountered with all early satellites was attitude instability due to enclosed liquids in a spinning and wobbling (precessing) vehicle. Usefully accurate prediction of energy dissipation within the liquid was needed. Vanyo & Likins (1972) provided an analytical model

that considered liquid in a precessing spherical cavity as if it were a rigid sphere separated from the cavity wall by an Ekman layer of viscous liquid. The analysis was originally derived as a possible limiting but probably unrealistic model. Comparison with energy dissipation tests (Vanyo & Likins 1971) showed, instead, it to be a very accurate model for real flows in spherical and nearly spherical precessing cavities. Various US and international satellite manufacturers have relied successfully on similar analyses and scaled energy dissipation tests (see Garg *et al.* 1986).

The same technique and apparatus were applied to luni-solar mantle precession to estimate energy dissipation within the liquid core. Experiments and analyses were able to set bounds on predicted energy dissipation using a cavity with $\varepsilon = (a-b)/a = 1/400$ ellipticity [see Vanyo & Paltridge (1981) and Vanyo (1984), where these results were scaled to Earth parameters]. A later paper (Vanyo 1991) attempted to integrate these and other ideas into a coherent model for flows necessary for a geodynamo. Kerswell (1993) derived criteria for the onset of turbulence in precession, analysed internal shear layers (Kerswell 1995) and calculated bounds on energy dissipation in precession (Kerswell 1996); Vanyo *et al.* (1995) published

photographs of internal flow structures using a transparent 1/100 spheroid; and Tilgner (1999a) analysed internal shear layers influenced by ellipticity and viscosity and derived an equivalent to the rigid sphere equation (Tilgner 1999b), but based on the Navier–Stokes equations, and deduced a negligible contribution of the Earth's solid core compared to that of the core–mantle boundary (CMB) as part of a general study of magnetohydrodynamic flow in precession. A brief summary of research described in this paper was presented at an American Geophysical Union special session in Boston, MA in May 1998 (Vanyo & Kerswell 1998).

2 LIQUID SPIN AXIS DISPLACEMENT

Displacement of the liquid spin axis from the cavity spin axis during steady-state precession was reported earlier in Vanyo (1991). That research used transparent globes with ellipticities of approximately $1/100$ and $-1/100$ during both prograde and retrograde precession. Figures here illustrate test results using a precisely machined globe with $+1/400$ ellipticity. The nominally 50 cm diameter cavity was machined to a $+1/400$ spheroidal shape to better than $\pm 25\,\mu m$. Ageing and water absorption may have compromised the accuracy to less than this value, although it is still within the known accuracy of the CMB shape.

Fig. 1(a) is a timed several second photograph of small buoyant sponges that mark the liquid spin axis. A gauge, as seen in Fig. 2(a), has its origin placed over the spin axis of the cavity. The photograph of the sponges locates the liquid spin axis (white dot) and shows it displaced from the cavity spin axis. In Fig. 1(a) the cavity spins at $\dot{\psi} = 200$ rpm about an axis displaced $\theta = 23°27'$ from the precession axis, here with precession velocity $\dot{\phi} = -0.056$ rpm. The photograph in Fig. 1(a) and the graph of Fig. 1(b) make use of the apparatus of Fig. 2(a). Precession with a 24 hr period using the apparatus in Fig. 2(b) yielded displacements too small to measure accurately. In Fig. 2(a) precession is clockwise, viewed from above, and spin is counterclockwise. The Earth provides counterclockwise precession in Fig. 2(b), so spin is clockwise.

In the remainder of this paper we usually write rpm for defining spin rate ($\dot{\psi}$) and period in minutes or hours for precession rate ($\dot{\phi}$). The Earth $\dot{\psi}/\dot{\phi}$ ratio is approximately 10^7. All experiments reported here are meant to approach this value using spin rates as high as possible and precession rates successively at 10 min, 100 min and 24 hr periods. The 24 hr period is achieved simply by fixing a spinning platform to the floor and then tilting it at $\theta = 23°27'$ to the Earth's rotation axis. Although the gauge was unable to measure accurately liquid axis displacement at 24 hr precession, the next section shows that significant phenomena are induced at this rate. An obvious question is whether any (all) rotating fluid tests fixed rigidly to a laboratory floor are affected by Earth rotation rate—for example, as a fluid rotor gyroscope (Wing 1963). It may be that laboratory experiments to measure thermal convection at the lowest measurable heat transfer rates are affected in this way.

A large number of photographs, as in Fig. 1(a), at increasing precession rates provide the loci of displacements of the liquid spin axis relative to the cavity spin axis. Fig. 1(b) shows three curves, one calculated using the rigid sphere ($\varepsilon = 0$) solution
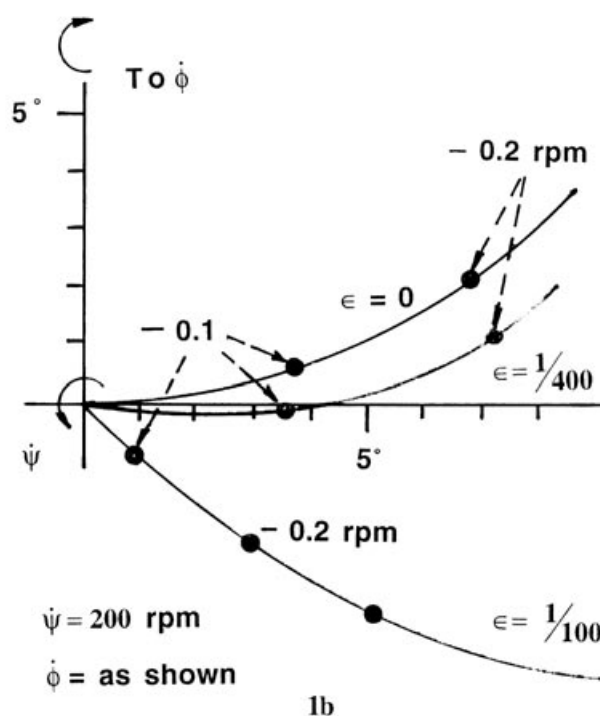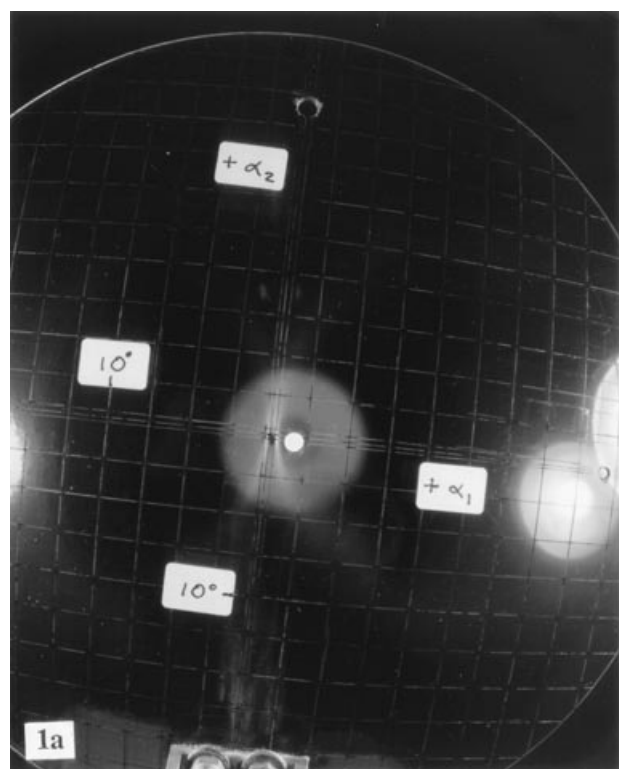

Figure 1. Photograph (a) shows a circular pattern caused by small buoyant sponges defining the liquid spin axis displaced from the cavity axis ($\dot{\psi} = 200$ rpm, $\dot{\phi} = -0.056$ rpm, $\theta = 23°27'$). A white dot marks its centre. (b) shows the loci of liquid axis displacements as a function of $\dot{\phi}$ for three cavity ellipticities ($\varepsilon = 0$, analytical; $\varepsilon = 1/100$, earlier research; and $\varepsilon = 1/400$, this research). Photographs can be viewed in colour in the online version of the journal (www.blackwell-synergy.com).
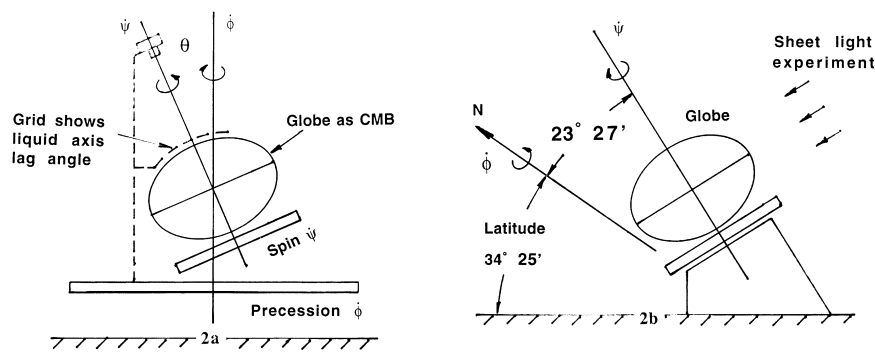
Figure 2. (a) depicts equipment capable of a wide range of $\dot{\phi}$ and θ, although limited to $\dot{\psi} = 200$ rpm All research using precession at 100 min, 10 min and shorter periods with $\dot{\psi} = 200$ rpm used this apparatus. (b) depicts a device rigidly secured to the floor and with its spin axis inclined $23°27'$ to the Earth's spin axis to provide a 24 hr precession period. It is designed to achieve $\dot{\psi} = 2000 \pm 1$ rpm, but various difficulties limit it at present to under 700 rpm.

of Vanyo & Likins (1972), a second for the present tests using the $\varepsilon = 1/400$ spheroidal cavity, and a third from Vanyo (1991) showing prior results using the $\varepsilon = 1/100$ cavity. The observation of interest here is the nearness of the 1/400 tests to the sphere calculations compared to the 1/100 tests. The slight dip beneath the horizontal axis is a function of ellipticity, but the net displacement from the cavity axis is due mostly to viscous coupling.

3 FLOW STRUCTURES AND FLOW RATES

The rigid sphere model, assuming a rigid core, predicts energy dissipation at the CMB. Maintenance of the geodynamo against resistive losses requires on the order of 10^{11} W, perhaps only a few per cent of the total heat generation within the Earth, but that energy must be supplied within the core—not just at the CMB. The following photographs and data illustrate the rigid sphere model to be only a first-order solution to precessing flows. Higher-order flows transport fluid in complex patterns within the boundary layer due to the relative velocity between the cavity and the 'rigid sphere', and axially parallel flows (cylinders) transport momentum to the core interior and keep the core interior precessing at the same rate as the mantle but lagging behind by a small angle. These flows are available to supply flow dynamics and energy to the geodynamo. Kerswell (1996), in an analysis of energy dissipation in precessing flows, supported this conclusion. He indicated that enough energy can be transferred from the precessing mantle to meet geodynamo energy requirements. These flows were first illustrated in Vanyo *et al.* (1995) and are continued here using a more relevant cavity ($\varepsilon = 1/400$) and over a more relevant parameter space. None of this negates the existence of other geodynamo mechanisms, e.g. core accretion, but the evidence here does infer that some portion of geodynamo needs, and perhaps most, are supplied by precession.

Except for replacing the 1/100 cavity of the earlier experiments with a precisely machined 1/400 cavity, a first set of tests retains the same parameters, $\dot{\psi} = 200$ rpm, $\theta = 23°27'$ and $\dot{\phi}$ at 10 min period. As before, fluoroscein dye is injected slowly into the boundary layer during steady-state precession, except now at more levels of latitude, that is, at 90°N, 60°N, 30°N, 3°N, 60°S and 90°S. In one experiment four different dyes were impulsively and simultaneously injected, 90°N (black), 60°N (red), 30°N (blue) and 90°S (yellow-green), during pre-

cession to define flow continuity between boundary flows and the interior cylinders. Visibility of the bottom (S) half is partially obstructed by support structure, and flow patterns passing N to S or S to N can usually be photographed best whilst in the top half. Some photographs depict a central cross-section through the liquid illuminated by a thin sheet of light; others use global exterior illumination. Use of a synchronized strobe light coordinated with a flash unit aids in selecting and photographing flows of interest. Flow rates were timed and recorded.

Additional experiments explored $\dot{\phi}$ at 100 min and 24 hr periods. The 100 min period tests were not pursued in detail, with the awareness that the precession axis (vertical in the laboratory at Santa Barbara, CA) was at the same time being precessed with 24 hr period by Earth rotation. Both the 100 min and the 24 hr tests produced easily observable data. Some tests at $\dot{\psi} = 695$ rpm and 24 hr $\dot{\phi}$ are included, but equipment modifications beyond present funding are needed to continue these and extend them to higher $\dot{\psi}$ (2000 rpm may be feasible). Earth $\dot{\psi}/\dot{\phi} = 10^7$, while 695 rpm $\dot{\psi}$ with 24 hr $\dot{\phi}$ gives 10^6. The Ekman number is 2×10^{-7} at these parameters. Retrograde drift of liquid relative to the cavity, that is, westward drift of the Earth's core relative to the mantle, is from right to left in the photographs for 10 min and 100 min precession, but from left to right for 24 hr precession (see Fig. 2).

A series of photographs (Figs 3–8) follow. Details are given in the captions. Each photograph shows ($\dot{\psi}$ rpm, $\dot{\phi}$ period, injection latitude) and time after injection, which can be used to estimate flow rates. Dyes are injected through thin tubing inside the metal band passing over the top half of the globe. The 90°N position on the globe in indicated by a white dot. The 60°N injection is also marked by a white dot. The 30°N is a black dot on a white background.

4 SOLID CORE: RELATIVE VELOCITY

Introduction of a solid core into the 1/100 cavity used in earlier tests provide data supporting existence of a cylindrical shear surface tangent to the solid core. The tangent cylinder tends to separate flows inside and outside this cylinder (see Fig. 9). The spherical solid core is fastened atop a thin rod fixed to the cavity bottom and kept from vibrating transversely with three thin wires. It cannot rotate relative to the cavity and provides no evidence of solid core to mantle rotation,
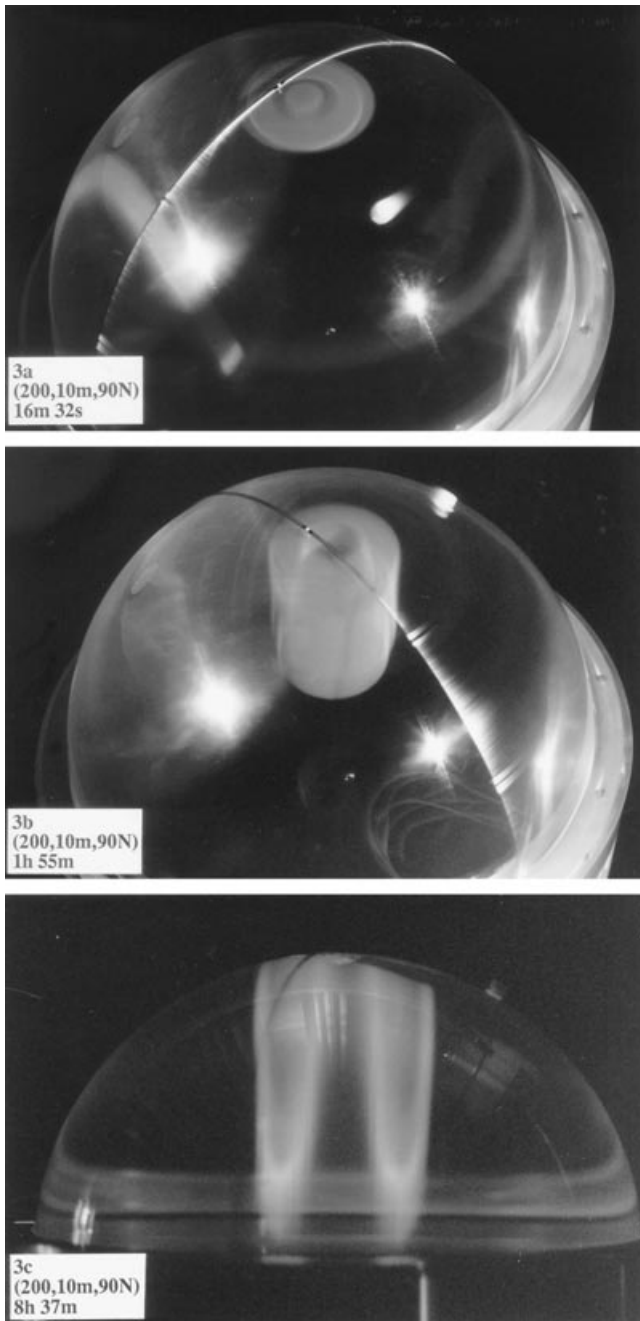
Figure 3. Each photograph shows ($\dot{\psi}$ rpm, $\dot{\phi}$ period, injection latitude) and time after injection. Notice in (a), after injection at 90°N, the central disk of dye surrounded by a clear ring and then a dye ring. In (b) the central disk has been displaced outwards by an uprising column of clear water, as will be verified in later photographs. Photograph (c) is illuminated by a thin sheet of light passing centrally through the cavity orthogonal to the camera. It illustrates cylinder structure and cylinder downward (upward) flow rate. The leading edge of the dye in (c) has a parabolic velocity profile within its parallel-walled cylinder flow structure.

although it does provide information on cylindrical structures and flow patterns. Before addition of the wires, transverse vibration of the solid core, such as might occur with translational oscillation of the Earth's solid core, produced flow structures similar to those of precession. The same effect was

observed with slight distortions of the thin walls of the spinning 1/100 cavity when filled with water and tilted 23°27′ from vertical. The 1/400 cavity is constructed with rigid walls and eliminates this phenomenon. The solid sphere and flexing wall results were briefly described at a Studies of the Earth's Deep Interior symposium by Vanyo *et al.* (1994).

Relative velocity ($\mathbf{V}^{\prime m}$) between the liquid core as a rigid sphere ($\boldsymbol{\omega}^{\prime}$) and the precessing mantle ($\boldsymbol{\omega}^{m}$) was described at an American Geophysical Union symposium by Vanyo & Lods (1994). The relative linear velocity at each point (P) when $\boldsymbol{\omega}^{\prime}$ is slightly less than $\boldsymbol{\omega}^{m}$ and displaced from it by a small angle β' is illustrated in Fig. 10(a). In the notation of this paper,

$$\mathbf{V}^{\prime m} = \boldsymbol{\omega}^{\prime m} \times \mathbf{R}, \tag{1}$$

$$V^{\prime m}(P) = \omega^{\prime m} R \sin \sigma, \tag{2}$$

where $\omega^{\prime m}$ is the magnitude of $\boldsymbol{\omega}^{\prime m} = \boldsymbol{\omega}^{\prime} - \boldsymbol{\omega}^{m}$, R is the CMB radius, $\sigma = \arccos(\cos\beta\cos\alpha\cos\lambda - \sin\beta\sin\alpha)$, $\beta = \beta'/2$, α is the latitude ($\pm$ from the mantle equator) to P and λ is the longitude east (from the plane containing $\boldsymbol{\omega}^{m}$ and $\boldsymbol{\omega}^{\prime}$) to P. The direction of $V^{\prime m}(P)$ clockwise from the west is

$$\gamma = \pi - \arcsin(\cos\beta\sin\lambda/\sin\sigma). \tag{3}$$

Interpretation is aided by noting that λ is the longitude from the plane containing $\boldsymbol{\omega}^{m}$, $\boldsymbol{\omega}^{\prime}$ and $\boldsymbol{\omega}^{\prime m}$, not from a longitude fixed on the mantle. Points P are not fixed to the mantle. In application to the Earth, $\boldsymbol{\omega}^{\prime m}$ presently points in a direction slightly west of the centre of the constellation Virgo and moves only at a precessional speed of about 0.1 arc s day^{-1}. Each day, geographical locations on the mantle at a latitude α are rotated past all λ points of the $P(\alpha, \lambda)$ pattern. Core liquid as seen by a mantle observer moves daily with circular motion at the poles, a sinusoidal-type motion at the equator, and ellipses at intermediate latitudes—fat ellipses near the poles and slender ellipses near the equator. An approximately dipolar field fixed in the core is sheared each day against a conducting lower mantle by these amounts and is twisted into rope-like structures as seen on the solar surface in sun spots (Babcock 1961), especially at mid- to high latitudes.

Fig. 10(b) illustrates the above applied to the mantle equator and pole using typical model parameters, here an equatorial westward drift at the CMB of 40 m day^{-1} and a linear displacement of 600 m between the liquid core and the mantle spin axes at the CMB. In this example, an observer located at point A on the mantle equator sees the liquid core equator 600 m north. After 12 hr the observer is at point B with the liquid core equator 600 m south, a 12 hr N–S displacement of 1200 m. Total N to S to N daily displacement is approximately 2400 m, and E to W displacement is 40 m. Because the relative orientation of the spin axes changes by only 0.1 arc s day^{-1}, during one day the pole of the core is displaced around a 1200 m diameter circle relative to the mantle (and vice versa). Total displacement is approximately 3770 m. Eq. (2) formalizes these relationships for all latitudes α.

Figs 3(a) and 7(b) illustrate circular motion at a pole. Dye injected at 90°N forms a circular streakline with each rotation ($\omega^{\prime} \approx \omega^{m}$). Swirls (ellipses) in boundary layer flows at mid-latitudes are seen in Figs 7(e) and (f) and 8(a) and (d). Large-amplitude small-wavelength (sinusoidal) patterns were observed after injections at 3°N but were difficult to photograph. A faint pattern is seen in Fig. 5(b) at low latitudes.
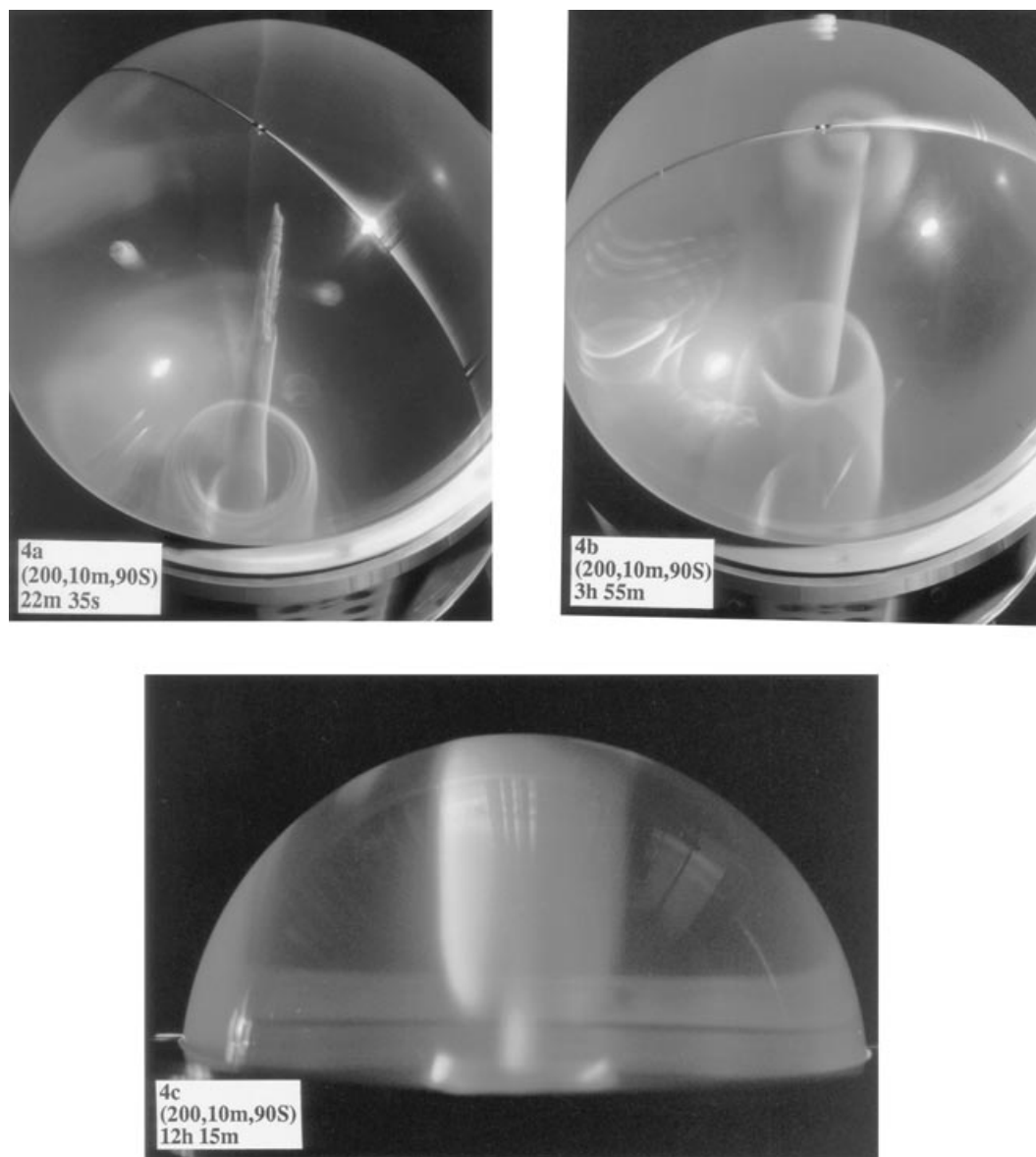
Figure 4. Compare these photographs to those of Fig. 3. Notice the pattern at the top surface of (b) and compare with Fig. 3(a). The phenomenon is more distinct in this 90°S injection because a larger amount of dye was used, the camera sees the interior free-surface interface, and injection at the pole from which the central column (spike) emanates permits quick migration of dye to the opposite pole. The large cylinder in (a) has a fine structure of 4 or 5 bands that diffuse into one in (b). The same pattern appears also in Fig. 7(f). In both Figs 3 and 4, the central column moves upwards, i.e. S to N.

5 EARTH MODELS: ENERGY DISSIPATION

Many of the consequences of precession and ellipticity are illustrated in the previous photographs and those of Vanyo *et al.* (1995):

(a) the liquid rotates as a nearly rigid sphere in a cavity with an ellipticity of 1/400;

(b) the liquid spin axis lags the cavity spin axis in precession;

(c) the liquid sphere has retrograde drift relative to the cavity;

(d) complex boundary layer flows exist because of both (b) and (c);

(e) a second-order flow exists as nested cylinders nominally axisymmetric with the liquid spin axis;

(f) alternate cylinders have slow prograde and retrograde angular velocities relative to the net rigid sphere motion;

(g) alternate cylinders have northward and southward internal flows;

(h) internal flows are laminar;

(i) energy dissipation is predicted accurately by the rigid sphere model (Vanyo 1984).

The rigid sphere model has been verified as a solution to the Navier–Stokes equations by Tilgner (1999b). During the past few years, he and Kerswell have analytically and numerically been able to reproduce many of the phenomena noted above.

All parameters and conditions applicable to the experiments reported here, in Vanyo *et al.* (1995) and in Vanyo (1984) are held to modern aerospace standards, typically within 1 per cent or better of stated values. These photographs and flow
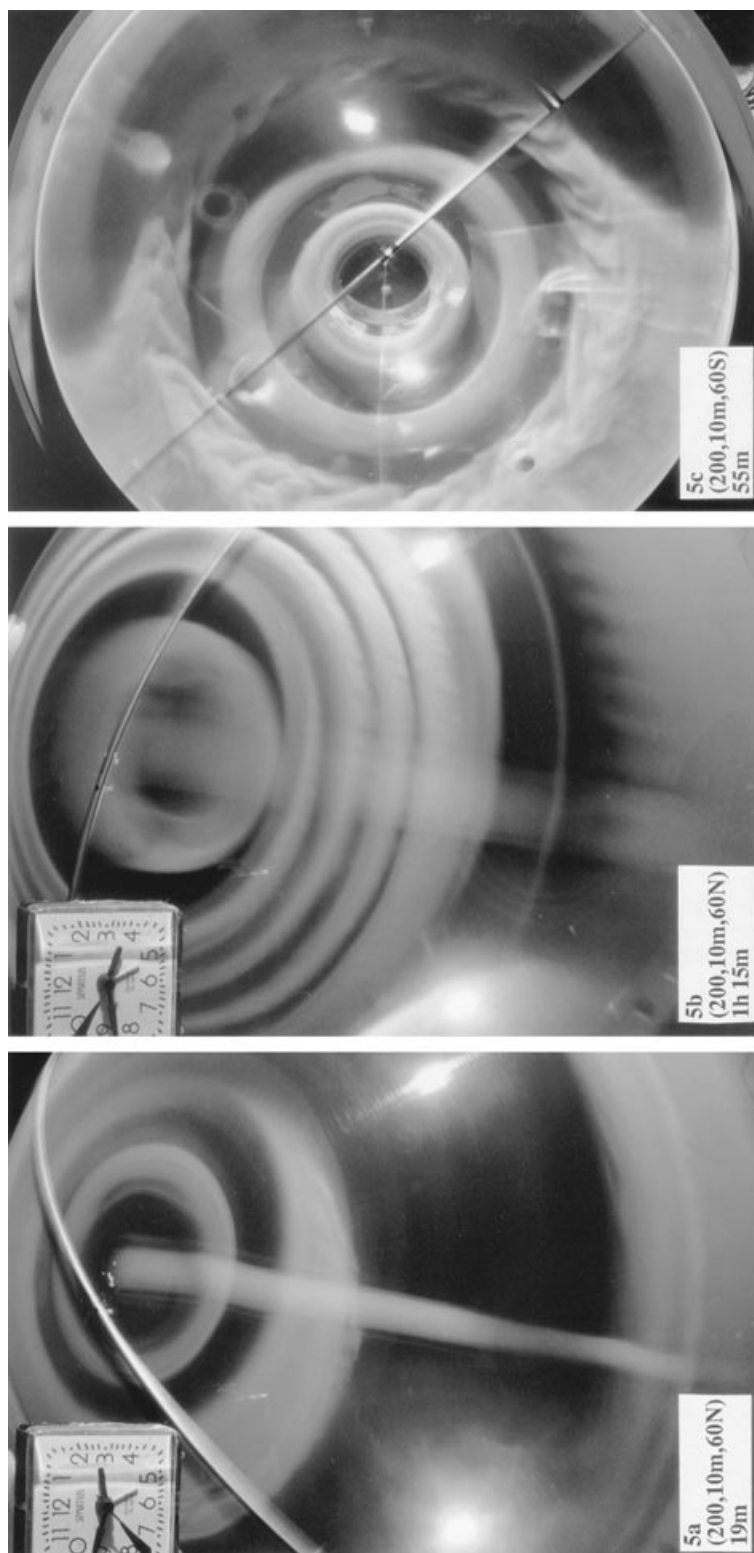
Figure 5. Compare these 60°N and 60°S injection photographs with those at 90°N and 90°S (Figs 3 and 4). Photograph (a) clearly shows a thin central column propagating downwards from N that is missing in Fig. 3(b). (b) shows cylinders that would fit inside the clear spaces in Fig. 3, and (c) shows a band with a set of periodic disturbances at about 60°S. The southern hemisphere now has the same pattern as the northern hemisphere of Figs 3 and 4. The experiment is symmetric, N and S, as is the Earth's core, except for its magnetic field, and there is no obvious reason why the pattern appears to reverse, north and south. Injection into the boundary layer at either 60°N or 60°S causes dye to be distributed throughout the boundary layer of that hemisphere. This is not seen in the 90°N or 90°S injections into the boundary layer, which tend to restrict dye propagation to regions near the poles. Injections at 3°N tend to stay in an equatorial band but do eventually distribute over the hemisphere. In all tests, there is little indication of dye migrating within the boundary layer past the equator.
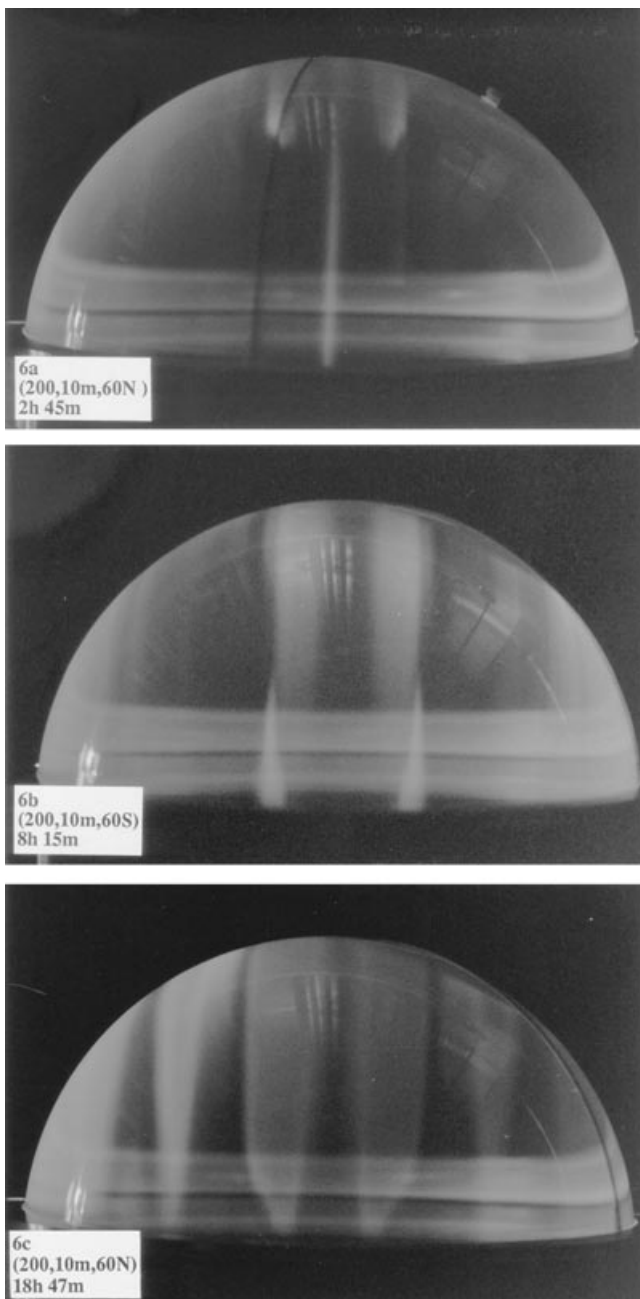
© 2000 RAS, *GJI* **142,** 409–425

Figure 6. These photographs are illuminated by a thin sheet of light as in Fig. 3(c) and illustrate cross-sections of the cylinder structures at the parameters and times shown. Photograph (c) shows patterns of dye nearly 19 hr after injection. In a similar test reported at an AGU seminar (Vanyo & Kerswell 1998), flow remained laminar during an entire 30 hr experiment. In that time the globe spun 360 000 times, precessed 180 times, and the liquid mass made 900 retrograde rotations relative to the cavity.

data can be used to verify proposed earth models by solving those models using these experimental parameters and conditions. Any proposed earth model that cannot reproduce these precisely known results should be used cautiously, or not at all, to predict Earth core phenomena. To complete the set of parameters given earlier, the test cavity used here is a generated spheroid produced by a computer-controlled lathe with a nominal accuracy of ± 0.0001 inches (2.5 µm). The spheroid geometry is

$a = 9.9283$ inches (25.218 cm) and $b = 9.9035$ cm (25.155 cm), with $\varepsilon = 1/400$. The acrylic cavity may have deteriorated to ± 0.0015 inches (40 µm) since manufacture. The test fluid is de-aired distilled water, and each dye is neutrally buoyant.

The experimental results can also be extrapolated, i.e. scaled, to estimate important Earth core phenomena. Accurate scaling requires geometric similarity, precise experiments and careful use of correct scaling, that is, appropriate and useful dimensionless parameters. The energy dissipation apparatus used for the $\dot{E}$ results in Vanyo (1984) matched energy dissipation predictions of the rigid sphere model, but more importantly was able to predict $\dot{E}$ accurately for two communication satellite programmes where attitude stability during orbit insertion was a potential difficulty.

In one, reported in Garg *et al.* (1986), a satellite manufactured by Ford Aerospace (now Loral) for India and launched on a Delta II vehicle of McDonnell Douglas (now Boeing) had been predicted stable by three separate analytical and numerical contractors—except their estimates varied by three orders of magnitude. Failure would cost some 150 million US dollars. The manufacturer built a scale model (1/10 size, 10 cm diameter) and dropped it spinning from a one-storey building. Extreme instability became obvious during the 1 s freefall, and the manufacturer awarded a contract to measure $\dot{E}$ using a scale model in the University of California, Santa Barbara (UCSB) fluids laboratory apparatus. These tests, like the 'drop test', predicted high $\dot{E}$ and instability, and the manufacturer repositioned sensors and antennae to compensate.

The liquid fuel tanks (fuel and oxidizer) were nominally spherical but contained large flexible vanes and plumbing to control and access fuel during zero gravity, and the tanks were only partially filled. 10 variables were reduced to seven by making them dimensionless, and a variety of analytical and experimental techniques were employed to match these. In-flight telemetry confirmed vehicle performance within about 15 per cent of scaled experimental $\dot{E}$ prediction; see also Vanyo (1974a) for details of a transformation from a 7-D experimental space to a 2-D analytical space.

In a second application, ERNO Raumfahrttechnik (Bremen) manufactured a communication satellite, also launched on a Delta II vehicle. Their tanks avoided the flexing vanes but also contained necessary propellant management structures. Tests were completed at UCSB with the support of ERNO engineers (Vanyo 1993). These tests indicated stability, and McDonnell Douglas later reported that in-flight telemetry confirmed a flight within 4 per cent of prediction. The ERNO tests used a proportionately larger 1/5 scale tank (22 cm diameter) to gain the advantages of the dependence of $\dot{E}$ on R^4 to R^5 and a better signal-to-noise ratio (Vanyo 1974b).

It may be unusual to include details as above, but it is necessary here to help validate the apparatus used to measure $\dot{E}$ in Vanyo (1984) and to validate our ability to scale complex precessional phenomena; see also the results of a recent Space Shuttle (STS84) experiment on the scaling of precessing liquid motion and energy (Chato *et al.* 1998). The Earth, as it is often modelled, is a simpler problem than these examples, and a prediction accuracy much less than the above would be satisfactory and useful. The remainder of the section will rely on the utility of the rigid sphere model and scaling methods.

The rigid sphere model of Vanyo & Likins (1972) is not a solution of the Navier–Stokes equations or even of a fluid flow. It is instead a solution of rigid-body dynamics (gyroscopics)
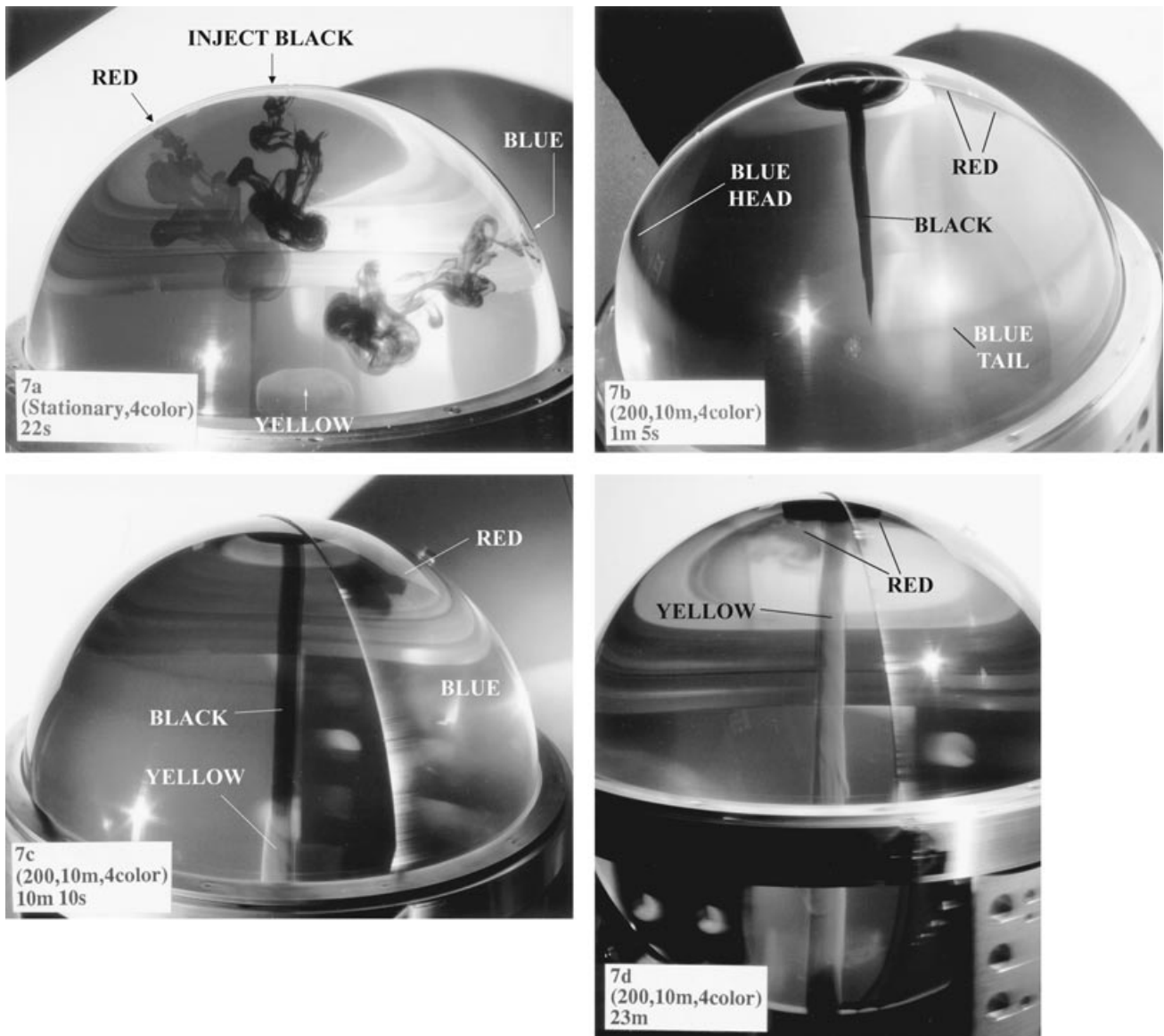
Figure 7. In this experiment, dye was impulsively injected simultaneously, at each of four latitudes. (a) shows dye propagation seconds after injection into stationary water for comparison with injection into spinning water. After achieving steady-state spin and precession, a similar injection illustrates dye propagation at progressive time increments. Injection is at 90°N (black), 60°N (red), 30°N (blue), and 90°S (yellow-green). The injections pierce the boundary layer and place dye directly into the cylinder structures, although angular momentum gradients severely limit transverse penetration at 30° and 60° injection. The objective is to define flow continuity among the N–S and S–N cylinder structures that interconnect through boundary layer flows. The yellow-green spirals in a left-handed sense as it rises in (c) and (d). It does not fluoresce in the narrow shadow near the bottom in (d), (f) and (h) and the interior black column is visible. All dyes are neutrally buoyant, black is ink, blue and red are food colours, and yellow-green is fluoroscein, which after a time dominates the other colours to end the experiment. In (b), the red and blue dyes have been transported 180° retrograde since injection. Fig. 7 is continued on the next page. Figs 7 and 11 are best viewed in four colours online (www.blackwell-synergy.com).

with viscous coupling. Separation between the sphere and cavity is assumed to be an Ekman layer with thickness $\sim(v/\omega)^{1/2}$ modified to be $(2v/\omega)^{1/2}$ to match measured energy dissipation rates. Angular velocity is taken as $(\dot{\phi}+\dot{\psi}\cos\theta)$ for the same reason, but neither are critical in application to the Earth's core. The rigid sphere model has the utility of having a simple algebraic solution from which most aspects of Earth core flows can be deduced with useful accuracy, including net motion of the liquid core, energy dissipation and relative velocity at the CMB. It does not, of course, model any phenomena due to ellipticity, but experiments and some analyses illustrate that these are minimal, including the generation of cylindrical flow

structures. Some flow within the cylinders may be driven partly by viscous relative motion at the CMB. Omission of a solid core, for this discussion, is supported by a derivation by Tilgner (1999b): '…the torque exerted by the inner core on the fluid in the shell with $r_i/r_0 = 0.35$ is only 2 per cent of the total frictional torque…'. In Figs 9(a) and (b) the solid core, fastened to and precessing with the cavity, does torque the liquid and force its spin axis to align more closely to the cavity axis. A model core, free to spin and precess in response to motion of the liquid, is not available.

The rigid sphere solution provides the three components of the angular velocity of the sphere (of liquid) relative to the
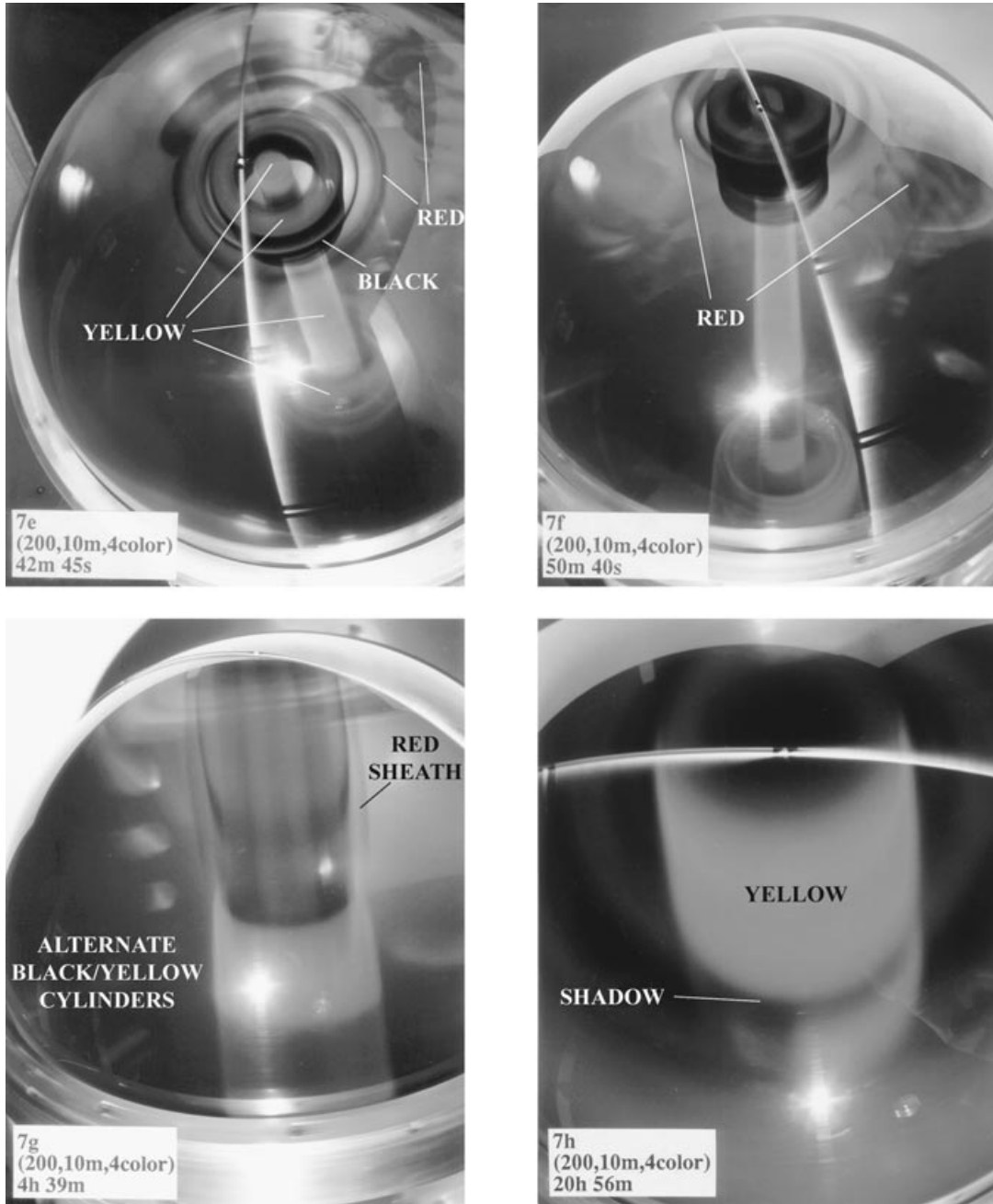
7e
(200,10m,4color)
42m 45s

7f
(200,10m,4color)
50m 40s

7g
(200,10m,4color)
4h 39m

7h
(200,10m,4color)
20h 56m

Figure 7. (*Continued.*)

precessing frame as follows:

$$\omega_1^\ell = -\frac{\zeta}{1+\zeta^2}\dot\psi\sin\theta,$$

$$\omega_2^\ell = -\frac{\zeta^2}{1+\zeta^2}\dot\psi\sin\theta, \tag{4}$$

$$\omega_3^\ell = \dot\psi\cos\theta.$$

In the same reference frame, the angular velocity of the mantle is

$$\omega_1^m = 0,$$

$$\omega_2^m = -\dot\psi\sin\theta, \tag{5}$$

$$\omega_3^m = \dot\psi\cos\theta.$$

The dimensionless parameter ζ has the form of an Ekman number,

$$\zeta = 5v/hR\dot\phi, \tag{6}$$

and is a measure of torque applied to the sphere and its angular momentum change.

The lag angle between ω^m and ω^ℓ can be computed using

$$\omega^\ell \cdot \omega^m = \omega^\ell \omega^m \cos\beta', \tag{7}$$

where β' is illustrated in Vanyo & Paltridge (1981). Energy dissipation at the sphere–cavity interface is

$$\dot E = \frac{\zeta}{1+\zeta^2} I^\ell \dot\phi\dot\psi^2\sin^2\theta. \tag{8}$$
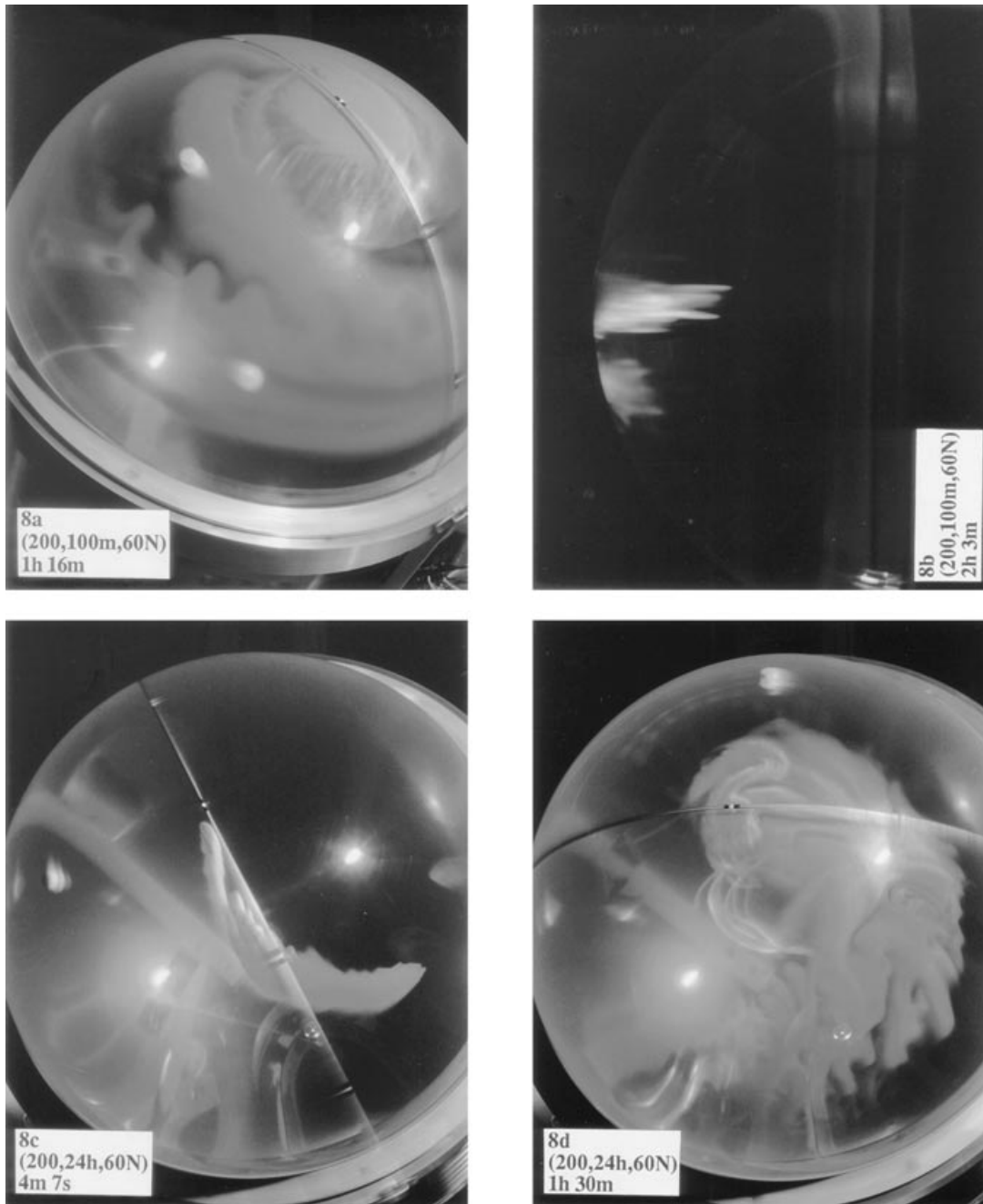
Figure 8. (a) and (b) show 100 min precession periods and (c) and (d) show 24 hr precession (Earth rotation used to generate precession). Both use $\dot{\psi} = 200$ rpm as before. Notice in (a) and (d) the slowly changing surface patterns at mid-latitude resembling ellipses. Dye here was injected very slowly into the boundary layer.

In earlier papers, the rigid sphere model was applied to the Earth's core by equating reported westward drift rates of surface magnetic anomalies of 0.2–0.3° yr^{-1} to the intrinsic retrograde (westward) drift of the sphere in the rigid sphere solution. Other model parameters are then computable using only this one identity and known values of R, $\dot{\phi}$, $\dot{\psi}$, θ and I^ℓ. Model parameters can also be computed by equating net heat loss from the Earth to energy dissipation predicted by the rigid sphere model. All other model parameters are then computable. Five equations, (9a)–(9e), were used when accepting westward

drift as the primary known quantity. Let

$$\Delta\omega = (\text{published estimate}),$$

$$\zeta = (\dot{\psi}\sin^2\theta/2\Delta\omega)^{1/2}, \tag{9a}$$

$$v = 2\zeta^2 R^2 \dot{\phi}^2/25\omega_s, \tag{9b}$$

$$h = (2v/\omega_s)^{1/2}, \tag{9c}$$

$$\xi = v/\omega_s R^2, \tag{9d}$$

$$\dot{E} = I^\ell \dot{\phi}\omega_t^2/\zeta, \tag{9e}$$

$$\beta' = \arctan[(\sin\theta)/\zeta]. \tag{10}$$
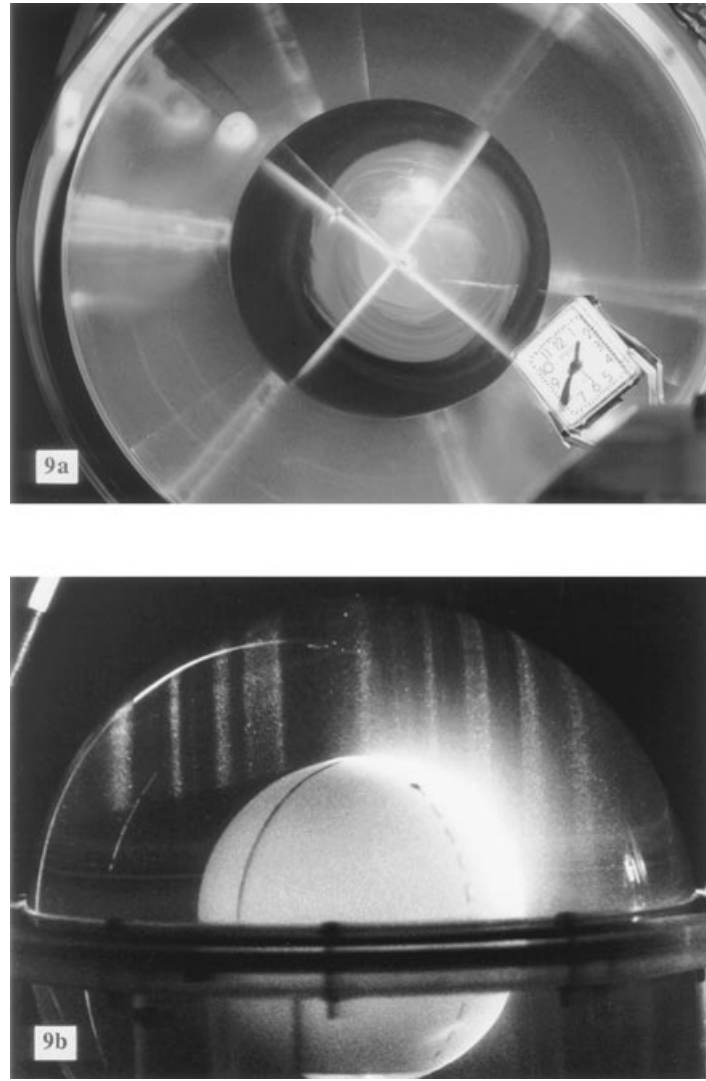
© 2000 RAS, *GJI* **142,** 409–425

Figure 9. (a) shows dye injection at 90°N into a spinning precessing cavity with $\varepsilon = 1/100$ and a solid internal sphere. Ratio of radii of the commercially available globes is 0.37. Compare with Earth solid core to CMB ratio of 0.35. After 45 min there is no evidence of dye migration outside the tangent cylinder. (b) shows cylinder structures illuminated using microscopic flakes as in Vanyo *et al.* (1995). The solid sphere is black with white lines in (a) and white with black lines in (b).
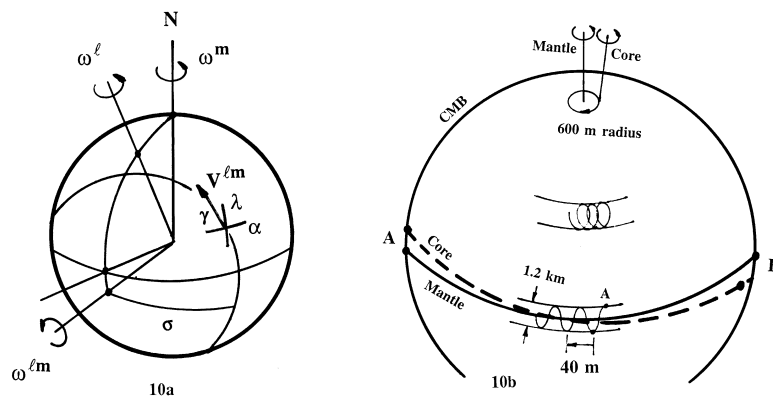

Figure 10. These diagrams illustrate CMB relative velocities. Clearly $\mathbf{V}^{\prime m}(\alpha, \lambda) = \boldsymbol{\omega}^{\prime m} \times \mathbf{R}$, where the $\mathbf{V}^{\prime m}$ are fixed in a reference frame with $\boldsymbol{\omega}^{\prime m}$ as a pole that moves only at the precession rate (25 800 yr period) as depicted in (a). (b) illustrates this motion as seen by an observer stationary on the mantle—he/she moves past the entire pattern each day at his/her latitude. Circular motion is observed by a polar observer; see e.g. Fig. 3(a). An equatorial observer sees a nearly sinusoidal relative motion as noted in the text; see Fig. 5(b) and note the periodic pattern of dye 'fingers' extending northwards from an equatorial band of dye. Figs 8(a) and (d) are tentatively identified as the mid-latitude ellipses depicted in (b); see also Figs 7(e) and (f).

© 2000 RAS, *GJI* **142**, 409–425

Here $\Delta\omega$ is the difference in magnitude of $\boldsymbol{\omega}^m$ and $\boldsymbol{\omega}^\ell$, ω_s is the secular component of the mantle angular velocity ($\dot{\phi} + \dot{\psi}\cos\theta$), ξ is the Ekman number, I^ℓ is the moment of inertia of a rigid liquid core (9.14×10^{36} kg m^2 based on Jordan & Anderson 1974) and ω_t is the transient component ($\dot{\psi}\sin\theta$).

We can make several comments about these simplified equations. In Vanyo (1984, 1991), eq. (9a) was in error, in that the 2 was omitted from the denominator, and the equations are valid only for $\xi^2 \gg 1$ and $(\Delta\omega/\dot{\psi})^2 \ll 1$ (both appropriate for the Earth's core). Eq. (10) was not included, and the value given for β' (0.01°) was based on a model using $\dot{E}$ as the known quantity after first solving for ζ in eq. (9e). At the CMB surface, an angular displacement of 0.01° equates to a linear displacement of 600 m.

Table 1 is based on the rigid sphere equations. The simplified equations (9a)–(9e) and (10) are used except for columns 1 and 4, where $\zeta = 1$ and 5.9, respectively. Eq. (8) clearly has a maximum at $\zeta = 1$. No value of core–mantle coupling in the rigid sphere model can produce a larger Earth $\dot{E}$ due to luni-solar precession than $\dot{E} = 3.0 \times 10^{16}$ W, i.e. of the order of 10^3 times that of the probable terrestrial heat flux. This is relevant in that the Gans (1972) estimate of $v = 0.6$ cs for core liquid leads to $\zeta = 0.83$ and excessive $\dot{E}$ rates assuming that liquid viscosity is the only coupling. A typical estimate of westward drift of magnetic anomalies of 0.25° yr^{-1} is taken as core drift for the column 2 earth model, and column 3 is an earth model obtained by equating $\dot{E}$ in eq. (9e) to a typical estimate of non-radiogenic terrestrial heat flow (3.1×10^{13} W) for comparison purposes. Column 4 applies to most of the photographs and data presented in this paper. Columns 5 and 6 are calculated for the 24 hr precession experiments ($\dot{\psi} = 200$ rpm and 695 rpm, respectively). Dimensionless scaling quantities for these experiments approach or equal those of the columns 2 and 3 earth models, although serious difficulties exist in attempting to reconcile the two earth models, as discussed in Section 6. For columns 1, 4, 5 and 6, $v = \mu/\rho$, where μ is the molecular viscosity. Columns 2 and 3 assume that μ is an 'effective' viscosity that represents all mechanisms opposing velocity gradients. Values of ζ and ξ are defined accordingly.

6 DISCUSSION

The column 2 model, based on an estimate of $\Delta\omega$, produces too much energy, and the column 3 model based on energy produces a $\Delta\omega$ less than the magnetic anomaly drift rate, both by 1–2 orders of magnitude. Modifications are needed in values for magnetic drift rate, effective viscosity, other coupling mechanisms, the Ekman number and energy dissipation rates and repositories.

Fluid viscosity was the only coupling mechanism relevant to the research of Reynolds and Ekman, and their numbers rely only on fluid viscosity as a coupling mechanism. Both the rigid sphere derivation and Tilgner's (1999b) derivation also assume coupling by a Newtonian fluid with $\tau = \mu \partial u/\partial y$. The rigid sphere model has been used previously to represent any and all mechanisms that might couple a core to a cavity, whether they consist solely of liquid viscosity, as in the experiments, or of some combination of fluid viscosity, eddy 'viscosity', form drag, magnetic coupling, pressure forces, etc. It is misleading to compute an Ekman number and an Ekman layer thickness using only viscosity as a coupling mechanism at the CMB when other mechanisms are also present. For example, Gans' (1972) value of v at the CMB is 0.6 cs, which yields $\xi \sim 10^{-15}$ and $h \sim 0.13$ m. A separation between the core and the mantle of 13 cm is meaningless. The numbers, to be relevant, need to be modified to include all coupling appropriate to the problem of interest. This approach can lead to more reasonable models, e.g. something like $\xi \sim 10^{-10}$ and $h \sim 100$ m, or even larger, where ξ now represents a ratio of 'coupling' to Coriolis rather than merely 'viscous' to Coriolis.

Total terrestrial heat flow from the Earth has been estimated at 4.2×10^{13} W by Sclater *et al.* (1980). Of that amount, Vacquier (1991) estimated that 1.14×10^{13} W is due to radiogenic sources in the crust. He attributed the balance to absorption of FeO from the mantle into the core and to secular cooling. Neither paper mentioned core accretion or the geodynamo. Geodynamo analyses rarely discuss total terrestrial heat flux. It may be incautious for researchers to reach a conclusion that a relatively small phenomenon such as the

Table 1. Fluid precession dynamics.

Parameter	Units	Earth core models			Units	Laboratory experiments		
		$\dot{E}$ max $\zeta = 1$	$\Delta\omega = 0.25°$ yr^{-1}	$\dot{E} = 3.1$ (13) W		200 rpm $\dot{\psi}$ 10 min $\dot{\phi}$	200 rpm 24 hr	695 rpm 24 hr
ζ	–	**1.00**	204	1.91(3)	–	5.87	846	1.58(3)
ξ	–	9.75(−12)	4.07(−11)	3.57(−9)	–	7.52(−7)	7.52(−7)	2.16(−7)
$\dot{\psi}/\dot{\phi}$	–	9.46(6)	9.46(6)	9.46(6)	–	2.00(3)	2.88(5)	1.00(6)
$\dot{E}/I^\ell\dot{\psi}^3$	–	8.37(−9)	8.20(−11)	8.75(−12)	–	1.31(−5)	6.50(−10)	1.00(−10)
$\Delta\omega/\dot{\psi}$	–	4.04(−2)	1.90(−6)	2.16(−8)	–	2.24(−3)	1.11(−7)	3.19(−8)
β'	radians	0.29	1.95(−3)	2.08(−4)	radians	6.70(−2)	4.71(−4)	2.53(−4)
v	m^2 s^{-1}	8.61(−7)	3.59(−2)	3.15	m^2 s^{-1}	**1.00(−6)**	**1.00(−6)**	**1.00(−6)**
h	m	0.16	32.8	307	cm	3.23(−2)	3.28(−2)	1.73(−2)
$\dot{E}$	watts	2.97(16)	2.90(14)	**3.10(13)**	watts	0.20	1.02(−5)	6.59(−5)
$\Delta\omega$	rad s^{-1}	2.95(−6)	**1.38(−10)**	1.58(−12)	rad s^{-1}	4.70(−2)	2.32(−6)	2.32(−6)
$D(\beta')$	m	9.93(5)	6.78(3)	724	cm	1.69	1.19(−2)	6.36(−3)
$V(\Delta\omega)$	m day^{-1}	8.86(5)	41.6	0.47	cm s^{-1}	1.18	5.84(−5)	5.85(−5)

The rigid sphere model, given R, I^ℓ, $\dot{\theta}$, $\dot{\psi}$, θ and the parameter in bold, determines the remaining parameters. D is displacement of the spin axes at the CMB due to β' and V is retrograde drift velocity at the equator due to $\Delta\omega$. Read 4.70(−2) as 4.70×10^{-2}, etc.

geodynamo can be immersed in so much energy and be unaffected. Estimates of geodynamo needs have varied from 10^9 to 10^{12} W, with a probable good estimate of 10^{11} W (Rochester *et al.* 1975). An estimate of 10^9 W is 40 000 times smaller than the total, and even Munk & MacDonald's (1975) estimate of 10^{12} W is 40 times smaller. The rigid sphere model using luni-solar precession can supply adequate energy for at least a major portion of non-radiogenic heat flux, with flow structures similar to those shown in the photographs supplying energy for the geodynamo. The difficulty may not be too little energy, but perhaps enough to account for geodynamo needs, mantle convection and tectonic activity.

This comparison of two earth models, one based on an estimate of westward drift and the other on terrestrial heat flux, implicitly infers that all data are reasonably correct, correspond to the same time period, and there is no time lag between the producing phenomenon and Earth surface appearance of data. Implicit also is that neither phenomenon varies significantly over time, yet global temperature is known to have extreme variations, even large variations over the last 3000 years (Singer 1999). Global temperature models typically rely on solar and atmospheric variations, especially greenhouse gases, to explain global changes. Variations in internal heat production and net heat loss from the Earth typically have not been considered in analyses of global warming or glaciation, yet there seems to be no justification for their omission. Channell *et al.* (1998), for example, present evidence for a strong correlation between magnetic palaeointensity records and variations of orbital obliquity and its effect on precessional forces in the core. They show obliquity (here θ) varying from $22°$ to $24.5°$ with a period of ~ 41 kyr. Energy dissipation ($\dot{E}$) is a function of ($\sin^2 \theta$), as in eq. (9e) (or see Vanyo 1973). The above change ($22°$ to $24.5°$) represents a change in $\dot{E}$ of 23 per cent. Changes in magnetic coupling at the CMB can produce even more significant changes in $\dot{E}$. Increased geomagnetic field intensity correlates with increased coupling and decreases in thermal energy production, and decreases in field intensity correlate with increases in thermal energy. Sudden increases in thermal energy production at the CMB, too rapid for conduction/convection to the surface, would cause transient episodes of melting and ablation of solids at the CMB and possibly the ICB.

Contrary to the Vanyo (1991) suggestion that fluid viscosity may be the major coupling mechanism at the CMB, values of effective v computed for columns 2 or 3 would be improved by including magnetic coupling. Toomre (1966) analysed magnetic coupling and concluded that is was negligible, although based on parameters different from those proposed here. Topographic coupling due to an irregular surface may not be relevant in that Vanyo (1984) reported minimal energy dissipation caused by deliberately formed smooth 'bumps' on an experimental cavity surface. As seen in Figs 8(a) and (d), complex and transient flows on a smooth 1/400 ellipsoidal surface are observed at slow precession rates. These are random enough to be tentatively classed as turbulence over an adequate time average. Pressure forces caused by ellipticity do appear to influence the nested cylinder patterns and some portion of the liquid axis departures from the cavity axis direction (see Tilgner 1999a).

In Table 1 (column 4) the dimensionless numbers indicate that some tests reported here and in Vanyo *et al.* (1995)

($\dot{\psi} = 200$ rpm and $\dot{\phi}$ with a 10 min period), while not useful for scaling directly to Earth core phenomena, do illustrate the consequences of precession and ellipticity and can be used to verify proposed analytical and numerical models when they are evaluated at test parameters. The liquid spin axis displacement angle (D) and retrograde drift velocity (V) are easy to measure for $\dot{\psi} = 200$ rpm and a 10 min precession period. Several photographs (e.g. Figs 3a, 4b, 5a and 7e), in addition to the data in Fig. 1(b), show $D = 1.7$ cm, which agrees exactly with the rigid sphere prediction in Table 1. Fig. 7(b) illustrates measurements for drift velocity (V). The blue and red dyes have progressed slightly over $180°$ in longitude in 65 s, or 130 s for a full revolution. Table 1, using $\Delta\omega = 4.70 \times 10^{-2}$ rad s^{-1}, predicts a full revolution in 134 s. Values of D for slower precession are too small to measure, e.g. $D = 0.12$ mm for a 100 min period. At slower precession, V is difficult to measure because relative velocity patterns quickly add too much complexity for a useful value, as in Figs 8(a) and (d). Dimensionless numbers for the test results using 24 hr precession approach, and sometimes equal, those of the two earth models. Fig. 11 illustrates flow structures with $\dot{\psi} = 500$ and 695 rpm and with 24 hr precession. Although not achievable with present apparatus and funding, tests with $\dot{\psi} = 2000$ rpm and $\dot{\phi}$ at 24 hr precession will compare favourably with an earth model that reaches a compromise between $\dot{E} \approx 3.1 \times 10^{13}$ W and $\Delta\omega = 0.25°$ yr^{-1}.

Other than refining and continuing these experiments to 2000 rpm with 24 hr precession and comparison tests using a sphere, future research may best be furthered with analytical and numerical techniques. Inclusion of a solid core free to spin and precess in response to fluid forcing appears not to be practical, perhaps not even feasible. Experiments to study magnetohydrodynamic phenomena have succeeded in improving our understanding of basic phenomena. It may be possible to impose an approximately dipolar magnetic field along the spin axis of Fig. 2(b) to gain some additional understanding.

Several observed phenomena in this research attract attention. Further research may be indicated.

(a) The experiment is symmetric, top to bottom, as is the Earth, except for its magnetic field. The pattern of alternate up and down cylinders should be reversible. After stopping and then starting a new test, they sometimes did reverse; for example, in Fig. 4(a) the central column (spike) moves up, in Fig. 5(a) it moves down, in Fig. 7(b) it moves down, and in Fig. 11(c) it moves up.

(b) CMB relative velocities, especially at high latitudes, consist of elliptical patterns that twist poloidal field lines traversing between the core and a conducting lower mantle in addition to adding magnetic energy by stretching lines. Twisting may bundle lines into magnetic ropes, as observed in sunspots (Babcock 1961), and provide spatial variations in the magnetic field at the CMB to augment coupling.

(c) The photographs in Fig. 9 illustrate the structure of a shear surface cylinder tangent to the solid core. Photographs of flow structures made visible by $90°$N and $90°$S injections of dye (see especially Figs 7g and h and 11f) demonstrate that a dominant flow is constrained to stay within a cylinder with diameter approximately equal to 0.35 that of the cavity, even without the inner core. Such coincidences are dangerous to interpret, but do raise the question of how N–S flows within a cylinder of solid core diameter might participate in solid
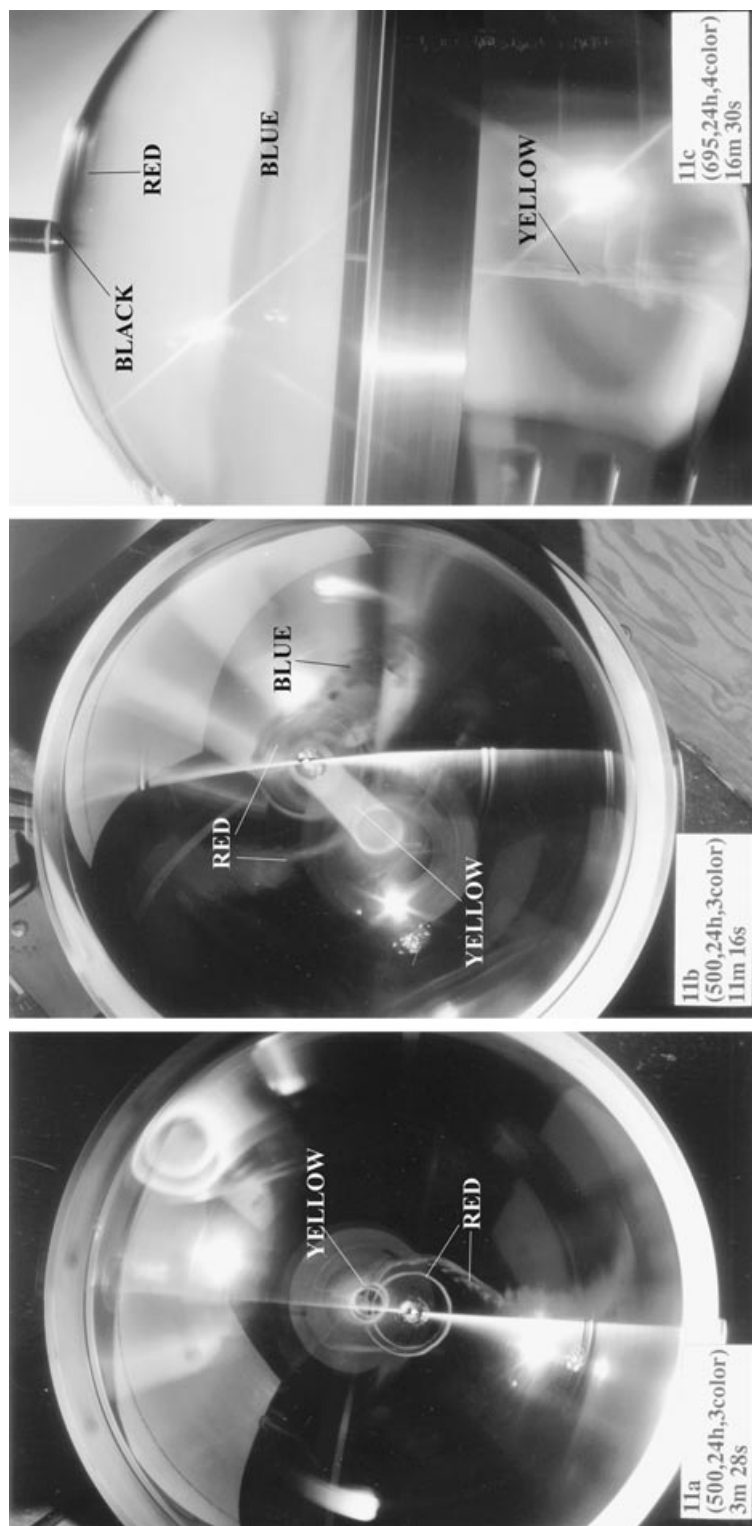
Figure 11. A preliminary set of experiments as in Fig. 7 was performed using the apparatus of Fig. 2(b). The same $\in\,=1/400$ cavity was used, but with ψ first at 500 rpm and then at 695 rpm, both with ϕ at 24 hr period. These conditions begin to approximate Earth core parameters. At $\psi=695$ rpm, $\psi/\phi=10^6$ versus 10^7 for the Earth, and the Ekman number is 2×10^{-7} versus 10^{-9}–10^{-15} for the Earth (depending on one's value for 'effective viscosity'). Flow structures form more slowly than those in Fig. 7 but are otherwise similar. The absence of black injection at 90°N for the 500 rpm test permits better observation of polar details. Injection of 2 ml of each dye for the 695 test helps illustrate retrograde drift of the 30°N (blue) and 60°N (red) injections. The leading edge of each (not shown here) drifts 180° in longitude in approximately 51 min, while the trailing edge of each moves only some 30°, creating the bands of blue and red dye as shown. (f) also shows that most of the axial flow occurs in a central cylinder with diameter approximately 1/3 of that of the globe. Note also that the southern injection of fluoroscein yellow now covers the southern hemisphere surface, while the northern injections (now blended to an opaque brown) remain in the northern hemisphere, except for the central axial flows. These higher speeds created several experimental difficulties and caused the photographs to be slightly blurred. A small cavitation bubble is seen in (a) and (b). In (c)–(f) the small cylinder on the globe spin axis provides water at atmospheric pressure to prevent cavitation caused by ullage created by globe expansion and by the 'O' ring sealing the two hemispheres being forced against its outer wall. At 695 rpm the 67 008 ml nominal globe volume is increased by less than 100 ml. Because a massive aluminium alloy ring constrains equatorial expansion, the increased volume is achieved by a nearly uniform expansion with little change in ellipticity. Tests were terminated because of the need for equipment modifications. Fig. 11 is continued on the next page.
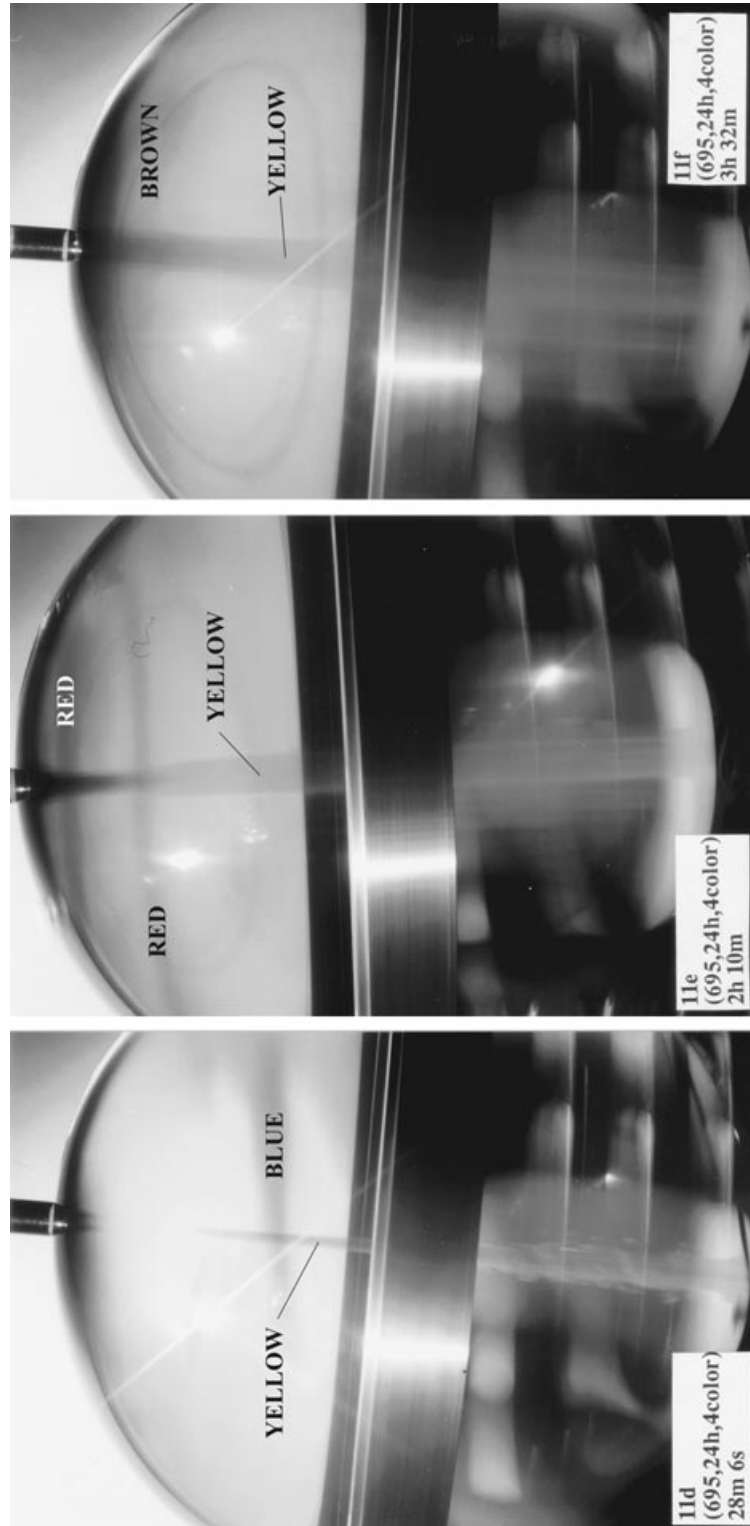
Figure 11. (*Continued.*)

core rotation and accretion, perhaps even maintaining or limiting the size of the solid core and/or its inertial stability. Preferential accretion at the poles or erosion at the equator will lead to inertial instability and possible inversion of the solid core.

(d) The discrepancy between the columns 2 and 3 earth models in Table 1 might be resolved by examining core–mantle coupling as flow between parallel streams with differing densities and viscosities. Lock (1951) examined this problem as a Blasius-type solution of the Prandtl boundary layer equations. His analysis used two parameters, U_2/U_1 and $\rho_2\mu_2/\rho_1\mu_1$. Shear stress and energy dissipation for Couette flow between rigid walls, as in the rigid sphere model, are functions of the velocity gradient ($\Delta u/\Delta y$). For free stream flow past a rigid wall, as the CMB might be modelled, shear stress is maximum at the wall. However, if the wall is soft and pliable, it yields and reduces the velocity gradient and energy dissipation, for example, wind blowing over water versus wind blowing over a solid surface; see also Schlichting (1987, Section IXg). Magnetic and/or turbulent coupling at the CMB have been included as additions to a homogenous and isotropic molecular viscosity in the rigid sphere model. Neither assumption is correct, and the inclusion of more realistic approximations is needed.

Rochester & Crossley (1987) and Lumb & Aldridge (1991) analysed whole Earth phenomena for evidence of core viscosity and core–mantle coupling. Research is available to support a range from Gans' estimate of 0.6 cs to 'soft solids' with rigidity ~ 0.01 times that of the mantle. The radius of the CMB is only known to an accuracy of several kilometres, much more than is needed for an h in Table 1 to provide a $\Delta\omega \sim 0.25°$ yr^{-1} without excessive $\dot{E}$. A smooth transition in ρ and μ from the lower mantle as a 'soft' plastic to the core as a near-Newtonian fluid (kept rigid by angular momentum gradients) over a distance < 1 km should be adequate. A model in Vanyo & Likins (1972) that uses a series of thin concentric spherical shells to provide a smooth transition from cavity to sphere, modified by increasing density and conductivity and decreasing viscosity of shells with depth (mantle to core), may provide a useful solution. Details are a part of ongoing research.

ACKNOWLEDGMENTS

REFERENCES

Babcock, H.W., 1961. The topology of the Sun's magnetic field and the 22-year cycle, *Astrophys. J.,* **133,** 572–587.

Busse, F.H., 1968. Steady fluid flow in a precessing spheroidal shell, *J. Fluid Mech.,* **33,** 739–751.

Channell, J., Hodell, D., McManus, J. & Lehman, B., 1998. Orbital modulation of the Earth's magnetic field intensity, *Nature,* **394,** 464–468.

Chato, D.J., Dalton, P.J., Dodge, F.T. & Green, S., 1998. Liquid motion experiment flight test results, *NASA,* TM-1998-208479.

Gans, R.F., 1972. Viscosity of the Earth's core, *J. geophys. Res.,* **77,** 360–366.

Garg, S.C., Furumoto, N. & Vanyo, J.P., 1986. Spacecraft nutational instability prediction by energy-dissipation measurements, *J. Guidance, Control. Dyn.,* **9,** 357–362.

Jordan, T.H. & Anderson, D.L., 1974. Earth structure from free oscillations and travel times, *Geophys. J. R. astr. Soc.,* **36,** 411–459.

Kerswell, R.R., 1993. The instability of precessing flow, *Geophys. Astrophys. Fluid Dyn.,* **72,** 107–144.

Kerswell, R.R., 1995. On the internal shear layers spawned by the critical regions in oscillatory Ekman boundary layers, *J. Fluid Mech.,* **298,** 311–325.

Kerswell, R.R., 1996. Upper bounds on the energy dissipation in turbulent precession, *J. Fluid Mech.,* **321,** 335–370.

Lock, R.C., 1951. The velocity distribution in the laminar boundary layer between parallel streams, *Q. J. Mech. appl. Math.,* **4,** 42–63.

Loper, D.E., 1975. Torque balance and energy budget for the precessionally driven dynamo, *Phys. Earth planet. Inter.,* **11,** 43–60.

Lumb, I.L. & Aldridge, K.D., 1991. On viscosity estimates for the Earth's fluid outer core and core-mantle coupling, *J. Geomag. Geoelectr.,* **43,** 93–110.

Malkus, W.V.R., 1968. Precession of the Earth as the cause of geomagnetism, *Science,* **160,** 259–264.

Munk, W.H. & MacDonald, G.J.F., 1975. *The Rotation of the Earth— a Geophysical Discussion,* Cambridge University Press, London.

Roberts, P.H. & Stewartson, K., 1965. On the motion of a liquid in a spheroidal cavity of a precessing rigid body, II, *Proc. Camb. Phil. Soc.,* **61,** 279–288.

Rochester, M.G. & Crossley, D.J., 1987. Earth's third ocean: the liquid core, *EOS, Trans. Am. geophys. Un.,* **68,** 481–483.

Rochester, M.G., Jacobs, J.A., Smylie, D.E. & Chong, K.F., 1975. Can precession power the geomagnetic dynamo?, *Geophys. J. R. astr. Soc.,* **43,** 661–678.

Schlichting, H., 1987. *Boundary-Layer Theory,* 7th edn, McGraw-Hill, New York.

Sclater, J.G., Jaupart, C. & Galson, D., 1980. The heat flow through oceanic and continental crust and the heat loss of the Earth, *Rev. Geophys. Space Phys.,* **18,** 269–311.

Singer, F.S., 1999. Human contribution to climate change remains questionable, *EOS, Trans. Am. geophys. Un.,* **80,** 183, 186–187.

Tilgner, A., 1999a. Non-axisymmetric shear layers in precessing fluid ellipsoidal shells, *Geophys. J. Int.,* **136,** 629–636.

Tilgner, A., 1999b. Magnetohydrodynamic flow in precessing spherical shells, *J. Fluid Mech.,* **379,** 303–318.

Toomre, A., 1966. On the coupling of the Earth's core and mantle during the 26,000-year precession, in *The Earth-Moon System,* pp. 33–45, eds Marsden, B.G. & Cameron, A.G.W., Plenum Press, New York.

Vacquier, V., 1991. The origin of terrestrial heat flow, *Geophys. J. Int.,* **106,** 199–202.

Vanyo, J.P., 1973. An energy assessment for liquids in filled precessing spherical cavities, *J. appl. Mech.,* **40,** 851–856.

Vanyo, J.P., 1974a. Transformation from a 7-dimensional experimental space for precessing fluid energy to a 2-parameter analytical space, *J. appl. Mech.,* **41,** 1128–1130.

Vanyo, J.P., 1974b. Cavity radius versus energy dissipation rate in liquid-filled, precessing, spherical cavities, *AIAA J.,* **11,** 261–262.

Vanyo, J.P., 1984. Earth core motions: experiments with spheroids, *Geophys. J. R. astr. Soc.,* **77,** 173–183.

Vanyo, J.P., 1991. A geodynamo powered by luni-solar precession, *Geophys. Astrophys. Fluid Dyn.,* **59,** 209–234.

Vanyo, J.P., 1993. *Rotating Fluids in Engineering and Science,* Butterworth-Heinemann, Stoneham, MA.

Vanyo, J.P. & Kerswell, R., 1998. The role of precession, solid Earth tides, and solid core motions in core dynamics and the geodynamo, *EOS, Trans. Am. geophys. Un.,* April Suppl., **79,** S71.

Vanyo, J.P. & Likins, P.W., 1971. Measurement of energy dissipation in a liquid-filled, precessing, spherical cavity, *J. appl. Mech.,* **38,** 674–682.

Vanyo, J.P. & Likins, P.W., 1972. Rigid body approximations to turbulent motion in a liquid-filled, precessing, spherical cavity, *J. appl. Mech.,* **39,** 18–24.

Vanyo, J.P. & Lods, D., 1994. MCB relative velocities in precessionally driven flows, *EOS, Trans. Am. geophys. Un.,* April Suppl., **75,** 120.

Vanyo, J.P. & Paltridge, G.W., 1981. A model for energy dissipation at the mantle–core boundary, *Geophys. J. R. astr. Soc.,* **66,** 677–690.

Vanyo, J.P., Lods, D. & Wilde, P., 1994. Precessing mantle, liquid core and solid core interactions, *4th SEDI Symp., Whistler, Canada,* abstract book, 62–64.

Vanyo, J.P., Wilde, P., Cardin, P. & Olson, P., 1995. Experiments on precessing flows in the Earth's liquid core, *Geophys. J. Int.,* **121,** 136–142.

Wing, W.C., 1963. Pros and cons on fluid rotor gyros, *Control Engineering,* **10,** 105–109.